Surface & Coatings Technology 255 (2014) 130–139

Contents lists available at ScienceDirect

Surface & Coatings Technology

journal homepage: www.elsevier.com/locate/surfcoat

Structural, chemical, optical and mechanical properties of Au doped Al – N sputtered coatings

N.M. Figueiredo [a,*], F. Vaz [b], L. Cunha [b], S.E. Rodil [c], A. Cavaleiro [a]

[a] SEG-CEMUC, Department of Mechanical Engineering, University of Coimbra, Portugal
[b] Center of Physics, University of Minho, Portugal
[c] Instituto de Investigaciones en Materiales, Universidad Nacional Autonoma de Mexico, Mexico D. F., Mexico

ARTICLE INFO

Available online 26 March 2014

Keywords:
AlN – Au
Au clusters
SPR
Decorative

ABSTRACT

This paper is focused on the structure, chemical composition, optical and mechanical properties of coatings consisting in an Al – N matrix incorporating different Au contents (up to 2.5 at.%). The Au was incorporated in the matrix atomically or in the form of very small nanoparticles (<1 nm). With the increase in the Au content both the refractive index and the coefficient of extinction were increased. The AlN matrix presented a crystalline wurtzite phase, stable up to 1000 °C.

With annealing at 400 °C the precipitation of XRD detectable Au nanoparticles was possible, originating SPR light absorption. The Al – N + Au coatings exhibited hardness values between 15 and 24 GPa, with no significant changes after the annealing treatments at low temperatures. These coatings are of interest to the decorative applications.

1. Introduction

Thin films containing metal nanoparticles are of interest to the electronics, glass, chemical sensing/detectors, biological, catalysis, semiconducting and computing industries. The main properties of interest are optical, catalytic, sorbents, electrical/thermal conductivity, antibacterial/biological, colour, photocatalysis, photochromic, electrochromic, photoluminescence, plasmon resonance shift and enhanced reactivity. The main purpose in this area is to produce and distribute nanoparticles with a specific size and shape either near the surface or embedded within a host matrix or a combination of both [1,2].

Composite systems of metal clusters and dielectric matrices have been produced by several methods, like melt quenching [3], ion implantation [4], sol–gel [2] and sputtering [5]. Among them, the sputtering method has been widely used due to its low cost, simplicity in process, flexibility in materials and controllability in size distribution.

Among the possible dielectric matrixes, Al-based compounds can be a good option due to their excellent mechanical and/or oxidation resistance properties. Usually, only aluminium oxide is exploited for these purposes, being given very little attention to aluminium nitride. Moreover, only thin films with reduced thicknesses are deposited, e.g. 200–500 nm, being thicker films not usually studied. Considering the particular system AlN-Au, in spite of AlN being largely deposited by sputtering for many different applications, only one study on the formation of AlN + Au nanocomposite coatings was found in the literature [6]. Considering other noble metals in AlN, Matenoglou and his co-workers studied recently [7] nanocomposite thin films consisting of a hard amorphous AlN matrix containing soft Ag nanocrystals grown by pulsed laser deposition (PLD). Very small (~3 nm) spherical silver nanoparticles of polycrystalline nature were obtained dispersed in the AlN matrix. The hardness of similar coatings was shown to be close to 15 GPa by Lotsari et al. [8].

In the present study, Al – N films were deposited with gold addition by reactive co-sputtering method using as reactive gas pure nitrogen. By means of incrusting Au pieces into the aluminium target, increasing Au contents could be achieved in the films. In order to try to obtain the desired metal particle size as-deposited coatings were annealed at increasing temperatures (increasing the segregation of metal clusters). The paper will be focused mainly on the sputtering conditions and on the structure, chemical composition, optical and mechanical properties of the coatings in order to understand their suitability for real applications in the decorative field.

2. Experimental details and data analysis

The coatings were deposited by reactive magnetron sputtering, from a rectangular aluminium target (15 × 15 × 1 cm^3, and 99.999% purity), using N_2 (99.999% purity) as reactive gas. In order to vary the Au content in the coatings, different numbers of gold pieces were incrusted in the erosion zone of the Al target. The used strategy consisted in drilling two circular grooves on the target (6 cm diameter), in each side of the erosion track, with 1 mm wide and 3 mm depth. Then, gold pellets (3 × 1 mm^2 of cross section) with varying lengths, from 1 up to 20 mm,

* Corresponding author. Tel.: +351 239 790 745; fax: +351 239 790 701.
E-mail address: nuno.figueiredo@dem.uc.pt (N.M. Figueiredo).

http://dx.doi.org/10.1016/j.surfcoat.2014.03.028
0257-8972/

and number (from 1 up to 10), were placed and distributed inside the grooves. Clear illustrations of this procedure can be found in [9]. The samples were placed in the substrate holder in front of the target not surpassing the zones defined with the incrusted Au strips. By measuring the height (depth) of the gold pieces before and after each deposition, it was possible to roughly account for the gold volume worn-out in each deposition and correlate it to the atomic concentration of the gold present in each coating.

An ENI RPG-50 asymmetric pulsed dc power supply was used, with a pulse frequency of 100 kHz and a duty cycle of 20%. The target power was set constant at 900 W (power density of 4 $W \cdot cm^{-2}$) and the deposition pressure was fixed at approximately 0.5 Pa. The substrate holder was neither biased nor intentionally heated and it was set to a constant rotation speed of 20 rpm. The target to substrate distance was fixed at 6 cm. The average N_2 mole fraction was 0.33, and for one sample the N_2 mole fraction was raised to 0.4.

Before deposition, an ultimate vacuum pressure better than 1×10^{-3} Pa was reached. All the coatings were deposited on silicon (111) plates. Prior to the deposition, the substrate surface was ion cleaned with an ion gun. The cleaning procedure included first an electron heating and afterwards an Ar^+ bombardment, for 10 min each (ion gun settings at 20 A, 40 V and substrate bias progressively increased to −70 V). The deposition time was kept constant at 90 min.

The thickness and the microstructure of the films were analysed by scanning electron microscopy (SEM) in a FEI Quanta 400FEG ESEM. The chemical composition of the coatings was determined by electron probe microanalysis (EPMA), using a Cameca SX-50 apparatus, equipped with wavelength-dispersive X-ray spectroscopy (WDX) capabilities, operating at 10 keV. The structure of the films was analysed by X-ray diffraction (XRD), using a Philips (PANalytical) diffractometer, operating with Co-K_α radiation in grazing incident configuration (GIXRD), with an incident angle of 2°. The XRD parameters, such as the peak position ($2\theta_0$), peak intensity and full width at half maximum (FWHM) were evaluated after fitting the diffraction patterns with a Voigt function.

The optical properties (transmittance spectra) of the coatings were studied using a UV–Vis-NIR spectrophotometer UV 3101 PC from Shimadzu, equipped with a slit of 1 mm. The films deposited on Si wafers were analysed as well using a Phase Modulated Ellipsometer Uvisel Jobin Yvon DH10 in the photon energy range of 1.5 to 5.0 eV, with steps of 0.005 eV, at 70° incidence angle. The ellipsometric data analysis was performed with the DeltaPsi™2 software supplied by Horiba Jobin Yvon.

X-ray photoelectron spectroscopy (XPS) experiments were performed in an ultrahigh-vacuum (UHV) system equipped with an X-ray source of Al-K_α. All the peak fittings regarding XPS were performed applying the Shirley background correction and using the proper area relation between doublets and a fixed spin-orbit splitting.

The hardness and reduced Young's modulus values of the coatings were evaluated by depth-sensing indentation technique, using a NanoTest platform from MicroMaterials, equipped with a Berkovich indenter. The applied load used was 5 mN, which allowed minimizing the influence of the substrate by keeping always the indentation depths inferior to ~10% of the coating thickness. At least 20 indentations were performed in two different places of the coating surface.

The samples were annealed at two different temperatures, 400 °C and 1000 °C, in a horizontal furnace with protective atmosphere (Ar). A heating rate of 30 °C/min and an isothermal period of 60 min were used, after which the furnace was turned off.

3. Results and discussion

3.1. Chemical composition

Table 1 shows the results of the chemical composition and thickness of the films, as a function of the amount of gold consumed during the deposition.

Fig. 1a) shows that there is a good relationship between the consumption of the gold pieces in the target and the Au content in the films. The measured gold concentration was in the range 0 to 2.5 at.%. Higher Au contents were not incorporated in the coatings since for the selected thicknesses this Au amount was sufficient to originate strong light extinction in most of the visible region (as discussed ahead in the optical analysis). For the coatings deposited with the same N_2 partial pressure, a small initial decrease in the deposition rate was found, followed by a progressive increase to values higher than the pure AlN. When depositing AlN films by reactive magnetron sputtering, the Al atoms sputtered from the surface of the Al target and reacting with activated N atoms or ions will form small AlN clusters. The presence of Au atoms during the film growth stage might have interfered with the incorporation of Al – N clusters in the film, provoking its desorption, and favouring the incorporation of isolated Al and N atoms. Since a significant part of the particles' flux arriving to the substrate is composed of Al – N clusters, for lower Au contents the thin films were deposited with slightly lower deposition rates than in the case of pure AlN. A further increase in the Au available in the target allowed higher deposition rates due to the higher sputtering yield of Au (when compared to AlN). The coating with higher Au content was deposited with higher N_2 partial pressure, which resulted in a lower deposition rate due to the higher target poisoning.

The Al/N ratio was, in all cases, close to the stoichiometric AlN, with a slight overvalue for nitrogen. The coating without Au exhibited the highest deviation from the stoichiometric AlN, with an N/Al ratio of ~1.2. Such a deviation was observed before by other authors (e.g. Tominaga et al. [10]) and can be attributed to depositions in compound mode, with excess of reactive gas. In all samples the presence of residual contents of oxygen was detected (<4 at.%), which was attributed to contamination effects either from the residual atmosphere or from the target. The over-stoichiometry of N is much less pronounced when increasing the Au content (Fig. 1b)), which allows speculating about the possible integration of Au atoms in the AlN lattice, perhaps occupying N positions. The affinity of Au for Al is much higher than that for N, its positioning as the first neighbour of Al being more favourable, with the tetrahedral arrangement in the AlN lattice. This is an admissible hypothesis since sputtered thin films are formed from individual atomic, molecular, or ionic species that have no solubility

Table 1
Deposition conditions, thickness results and chemical analysis for the Au-AlN composites.

Ref.	Au used on Al target		Thickness (μm)	D.R. (nm/min)	Atomic % (EPMA)				Al/N
	Total length (mm)	Volume worn out (mm^3)			Au	Al	N	O	
AlN-0	0	0	2.0	22.2	**0.0**	44.3	50.9	4.8	0.87
AlN-0.5	10	4	1.6	18.3	**0.9**	46.6	49.8	2.6	0.94
AlN-1	20	4	1.7	18.9	**1.2**	46.5	49.1	3.3	0.95
AlN-1.5	30	6	2.0	22.2	**1.6**	45.7	48.8	3.9	0.94
AlN-2	30	18	2.6	28.3	**2.0**	47.0	48.1	2.9	0.98
AlN-2.5[a]	30	15	1.8	20.0	**2.5**	47.1	48.5	1.9	0.97

[a] In this case the partial pressure of N_2 was set to higher values.

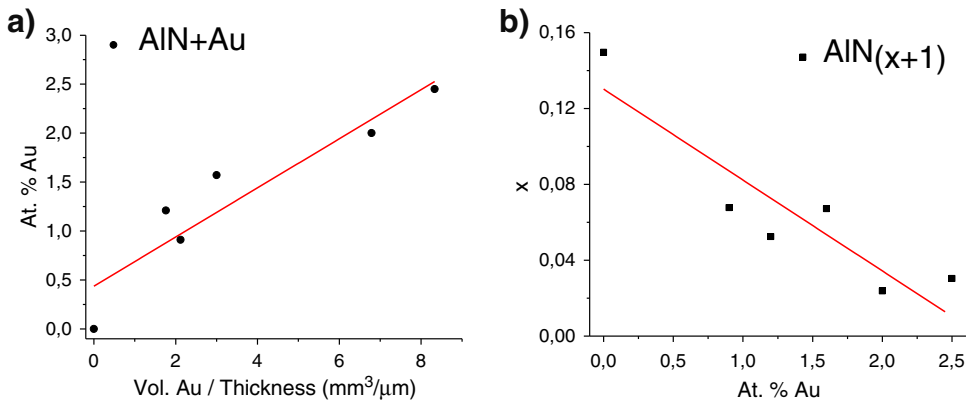

Fig. 1. a) Volume of gold sputtered normalized to the film thickness versus the atomic Au concentration determined by EPMA. b) Deviation from the stoichiometry in the AlN_{1+x} matrix with the Au content (the trend lines are only a guide for the reader).

restrictions in the vapour phase, and thus the solubility conditions between different materials on co-deposition are considerably relaxed [11]. Although Au is usually viewed as an inert material, its increased reactivity when in the form of very small nanoparticles has been recently demonstrated and is now an accepted fact [12]. Thus under appropriate deposition conditions, it is possible to sputter deposit Au–Al-based solid solutions [13].

3.2. Structure and microstructure of the coatings

The microstructure of the coatings was analysed by SEM and the structure of the coatings was analysed by XRD.

In Fig. 2 cross-sectional SEM images of the Au-AlN nanocomposites are shown. All the films, including the one deposited with higher deposition pressure, have dense columnar microstructures, which are typically characteristic of the transition region of the Thornton model [14].

AlN crystallizes in the equilibrium hexagonal closed packed (wurtzite 2H polytype, lattice constants: $a = 3.11$ Å, $c = 4.98$ Å) structure. AlN prefers to grow with closed-packed planes aligned normally to the growth direction [15]. It has been reported that AlN films show (100) preferred orientation at low nitrogen concentration and, with the increase of this parameter, the films tend out to be more randomly orientated, leading finally to *c*-axis (002) oriented films with further increasing in the nitrogen concentration [16]. However, inverse trend was also observed by other authors [17], i.e. they found a progressive decrease of (002) intensity when partial pressure of N_2 was increased during the deposition. Using a RF sputtering system,

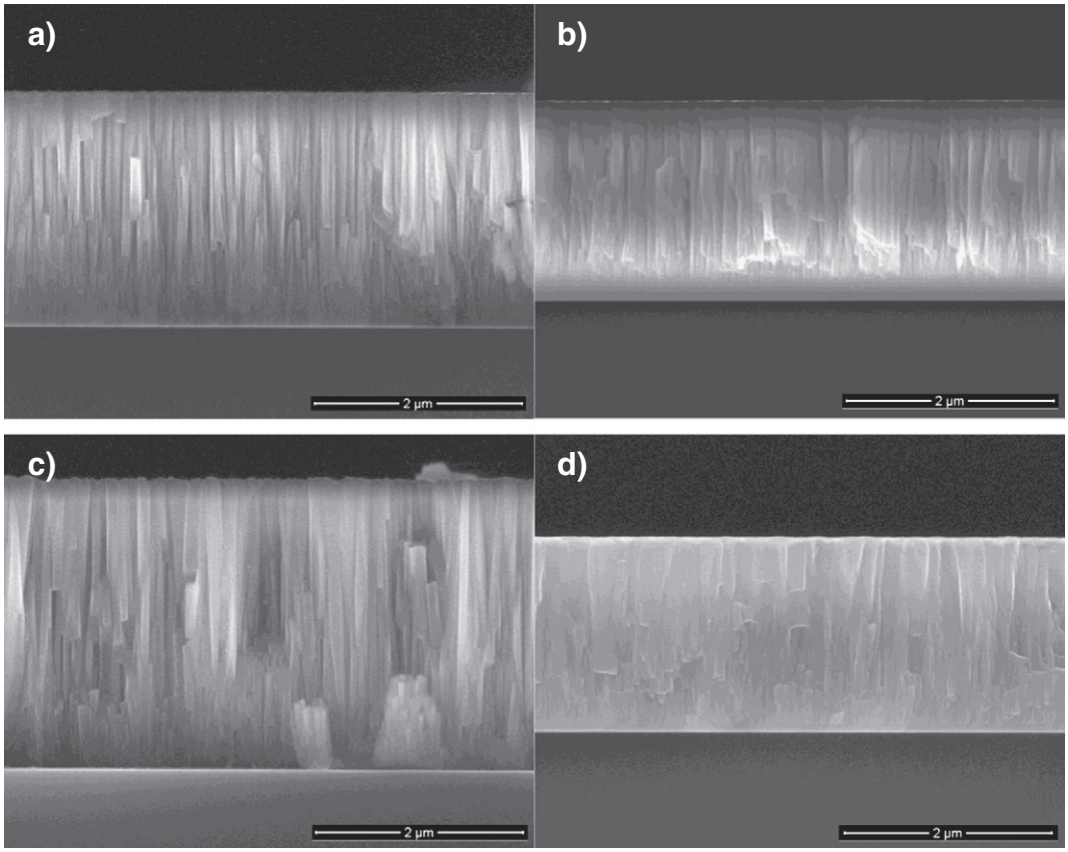

Fig. 2. SEM images of the as-deposited Al – N + Au films with different Au contents: a) 0 at.%, b) 1.2 at.%, c) 2.0 at.%, and d) 2.5 at.%.

Bienk et al. [18] observed orientation changes in the films from (001) to (101) with increasing power. However, using the same system but another setting they observed the opposite trend of the film orientation from a mixture to a (001) orientation with increasing pressure. Nevertheless, in both cases, at low deposition rate conditions a (001) orientation was obtained while at higher deposition rate conditions other orientations were observed. A. Rodríguez-Navarro et al. [19] found that for low deposition rate conditions the preferred orientation is after (001) while for higher deposition rates the (101) orientation is observed. Ion bombardment processes greatly influence the properties of the films, inducing adatoms mobility, assisting on the arrangement of the arriving growing units and selecting the orientation of crystal grains. Xu et al. [20] concluded that when the deposition conditions are favourable to the formation of AlN clusters in the gas phase thin films with (100) preferred orientation are grown, whereas the (002) orientation is favoured when the arriving species are mainly Al and N atoms.

All the as-deposited Au-AlN films presented diffraction peaks characteristics of the hexagonal structure of the AlN (Fig. 3a)), with the main intensities for the (002) or the (101) planes, being also detected the (102) diffraction peak. In spite of the use of glancing mode, the fact that different intensities were found in the samples, with and without gold, suggests that preferential orientations could be related either with the different Al/N ratios or to possible influences of Au incorporation in the adatom mobility of the arriving species to the growing film [16,18–20]. In fact, the presence of Au atoms during the film growth stage has most probably interfered with the incorporation of Al – N clusters in the film (as discussed before). And this favours the incorporation of isolated Al and N atoms, which in turn favours the (002) orientation. Subsequently, the higher deposition rates of the samples with higher Au contents favoured the growth of crystallites with a mixture of orientations, with special emphasis on the (002) and the (101).

No diffraction peaks corresponding to the gold phase were detected in the as-deposited samples, even for the sample with the highest gold content (2.5 at.%). These results point either to the presence of very small Au aggregates (<1–2 nm) in the AlN matrix or to the atomic integration of Au atoms on the lattice of the wurtzite structure, eventually in substitution of the Al atoms (as it was suggested above from EPMA result analysis).

Regarding the annealing treatments, at 400 °C (Fig. 3b)) broad peaks of the (111) Au diffraction were detected for all the samples containing Au. For the sample containing 0.9% Au this feature was clearly distinguishable due to the absence of the (101) diffraction of the hexagonal AlN in the original as grown sample (Fig. 3a)). For all the other samples the (101) AlN diffraction peaks have become asymmetrically broadened, at the higher angles, near the position of the (111) Au diffraction. The diffractograms of the samples annealed at 400 °C can thus be interpreted as the result of nanoparticles of gold dispersed in a crystalline Al – N matrix.

For the highest annealing temperature (1000 °C) the partial delamination of the films has occurred, which contributed to a worse definition of the XRD's spectra. The diffractogram of the sample containing most Au content is shown in Fig. 4. Again, a strong asymmetry of the (101) peak is observed which, after deconvolution, gives rise to a broad peak at the (111) position of gold. An interesting point coming from the analysis of Fig. 4 is the almost unchanged state of the FWHM of the AlN peaks after annealing at 1000 °C, showing the very high thermal stability of this phase, even with a nanocrystalline grain size.

Fig. 5 shows the lattice parameters, a and c, of the h-AlN phase, values calculated from the (002) and (101) peak positions. An increase in the Au contents in the coatings promotes an increase in the lattice parameters. This shows that the films are under increasing compressive stress [21]. However, the typical strong unilateral elongation in the c direction is not observed. Both the lattice parameters a and c increase with the Au content, such as the c/a ratio (varying between 1.606 and 1.613) is maintained very close to the one of the pure AlN of the standard ($c/a = 1.601$). The trend in the lattice parameters, along with the absence of Au diffraction peaks, suggests that the Au is being accommodated either as very small precipitates (<1–2 nm) or as substitution in h-AlN grains, or as both. After annealing at 400 °C there is a recovery of the lattice parameters due to a thermal stress relief mechanism combined with the precipitation of XRD detectable Au clusters. After annealing at 1000 °C, the lattice parameters recovered to values close to the equilibrium ones [22], whatever the Au content in the film was.

3.3. Chemical bonding

The chemical state and distribution of the elements in the coatings were assessed by XPS in order to try to understand the distribution of the Au atoms in the matrix and the possible interactions that occur between Au and the matrix elements, before and after applying thermal treatments.

The charging effects that frequently arise during XPS measurements were corrected at the surface by assuming that the C-C bond from the contamination layer had a binding energy (BE) of 284.7 eV in the C 1s spectrum. As for the XPS depth profile curves, a reference was made to the Al – O bond peak detected at the surface of the O 1s spectrum (with BE close to 531.5 eV), arising from the incorporation of oxygen of contamination.

The elements that were analysed by XPS to characterize the Au – Al – N system were the Al 2p and N 1s lines, for the matrix elements, and the Au 4f lines for the gold. The oxygen present in

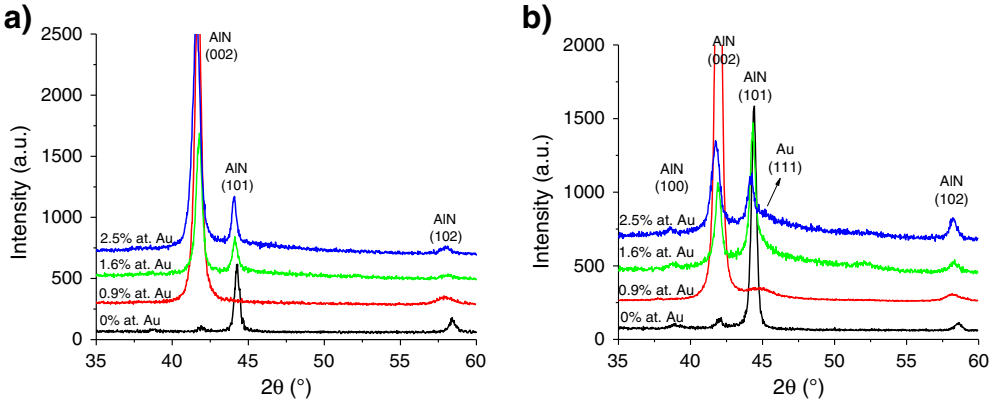

Fig. 3. GIXRD patterns of the Al – N + Au films with different Au contents a) before and b) after thermal annealing at 400 °C.

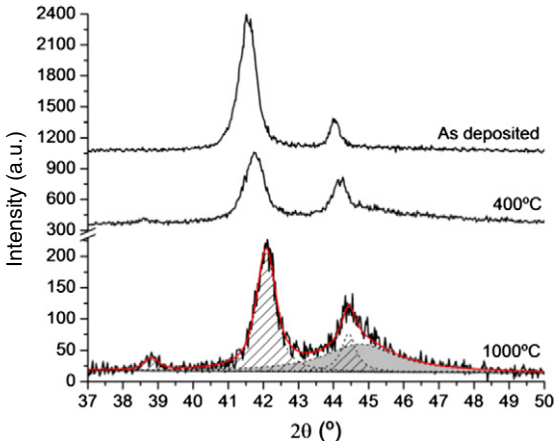

Fig. 4. GIXRD pattern of the Al – N + Au (2.5 at.% Au) sample before and after the thermal annealing treatments (at 400 °C and 1000 °C).

the matrix, resultant of contamination, was also characterized by the O 1s lines.

The intensity ratios utilized during peak fittings were 4:3 for the $j = 7/2$ and $j = 5/2$ components of the Au 4f doublet and 2:1 for the $j = 3/2$ and $j = 1/2$ components of the Al 2p and Si 2p doublets. Furthermore, the spin orbit splitting of the Au 4f and Al 2p levels was fixed with a separation energy of 3.65 eV [23] and 0.4 eV [24], respectively.

3.3.1. As-deposited samples

For all the as-deposited samples, in the N 1s spectrum (Fig. 6a)) only one peak was observed, located around 396.6 eV, here attributed to the Al – N bonding, as it is confirmed by the major peak detected in the Al 2p spectrum (Fig. 6b)) with a BE value close to 73.3 eV, and in accordance to what it is reported in literature by several authors [23,25,26]. A minor shoulder in the higher BE region is also detected in the Al 2p spectrum around 74.6 eV, responsible by the small asymmetry in the curve, arising from the Al – O bonding, suggesting that the oxygen incorporated during the sputtering process is preferentially bonded to the Al atoms. This bond is also confirmed in the O 1s spectrum (Fig. 6c)) by the presence of one peak close to 531.6 eV.

The Au 4f XPS spectrum (Fig. 6d)) of the Au doped samples (with 0.9 and 2 at.% Au) revealed only one peak with BE close to 84.8 eV and a full width at half maximum (FWHM) of ~1.8 eV. This is a significantly higher BE value than the one expected for the bulk Au (representing a +0.8 eV shift). This could indicate an emission from a strongly electron-withdrawing chemical environment, which could be the case

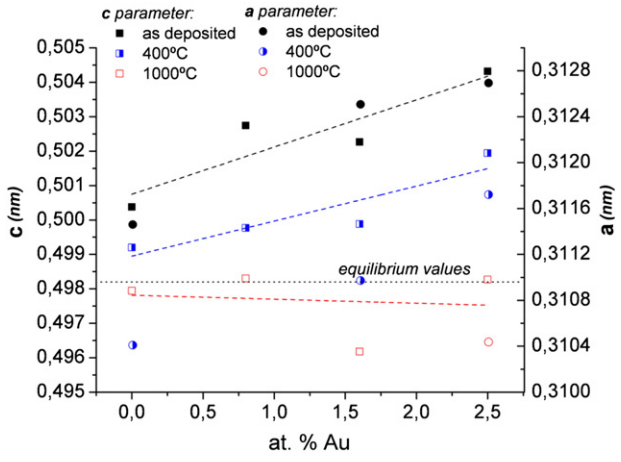

Fig. 5. Lattice parameters of Al – N + Au films with different Au contents (the trend lines are linear fits to each set of *c* data, and are only meant to be a guide for the reader).

of isolated atoms or small nanoparticles of gold surrounded by the matrix. We observed before similar shifts (up to ~1 eV) and linewidth broadenings (up to ~2 eV) for the case of composite thin films consisting of small nanoparticles of Au embedded in an Al_2O_3 matrix, obtained by a similar reactive magnetron co-sputtering process [13]. Shortly, due to the presence of size effects in the Au aggregates (discretization of the conduction band), there is a reduction in the screening of the core holes, that is also not compensated by the surrounding medium in the typical lifetime cycle of a photoemission process, thus resulting in positive BE shifts. These shifts arise only for nanoparticle's sizes below 3–4 nm, being directly dependent on the clusters size. Thus this shifted peak is hereby attributed to the presence of either very small Au clusters (dimensions <0.5–1 nm) or individual Au atoms in the matrix. This result agrees well with the XRD analysis, where no Au diffraction peaks were detected in the as-deposited samples.

3.3.2. Annealed samples

Two sets of samples were also analysed after thermal annealing, one without Au and another one containing 0.9 at.% Au. For the sample without Au, annealed at 400 °C, there were not any visible changes in the spectra regarding peak shapes, areas and positions. The area of the oxygen peak in the O 1s spectrum (from Al – O bond) diminished with the profile depth until attaining a stabilized profile on the last two curves of the measurements (120 and 150 s of sputter time), having occurred the inverse phenomenon with the total areas of the N 1s and Al 2p spectra. This suggests a surface oxidation of the thin film with the temperature.

The sample with 0.9 at.% Au was analysed by XPS after two different thermal annealing treatments, one at 400 °C and another at 1000 °C. For the sample annealed at 400 °C the main change that took place regarding the as-deposited sample occurred in the position of the two peaks associated with the Al – N bonding (in the Al 2p and in the N 1s spectra, Fig. 7b) and a) respectively), both presenting small positive shifts of ~0.1 eV. Furthermore, the Au-Au bond peak did not change its position in the Au 4f XPS spectrum (Fig. 6d)), suggesting that the small gold clusters did not increase in size (bigger clusters are expected to originate smaller shifts due to relaxation effects). Since the XPS is only probing the surface of the thin films (in the specific case the first ~10–20 nm) and, on the other hand, XRD detected Au clustering, Au precipitation should have been occurring in the bulk of the coating and/or near the interface between the film and the substrate, as we have also concluded previously for the Au – Al – O system [13]. Again, a surface oxidation of the thin film was observed since higher contents of oxygen were detected in the top layers.

The small positive shift that was observed in the two main constitutive elements of the matrix, Al and N, regarding the Al – N bond peaks, could indicate an increased tendency for an electron transfer from the nitride matrix to the gold nanoparticles, that could take place in the interface between the gold clusters surface and the nitride specie. We can speculate that with the increase in temperature a better homogenization of the shape of the clusters towards the spherical geometry is expected, driven by the minimization of the surface energy. This should promote an increase in the average coordination number of the Au atoms and thus the reactivity of the clusters should diminish [12]. Therefore the electronic transition from the matrix to the Au becomes now more feasible.

For the sample annealed at 1000 °C, a similar variation in the peak's position corresponding to the Al\ – N bonding as in the 400 °C annealing was observed (+0.1 eV in both the Al 2p and N 1s spectra). Again, the Au 4f peak associated with the gold clusters did not shift to lower BE, as it would be expected in the case of cluster growth. However, as can be observed in Fig. 7 (spectra obtained with similar ion etching times), an increased oxidation state with the annealing temperature is obvious, resulting in the progressive depletion of Au from the surface with the increase of the annealing temperature.

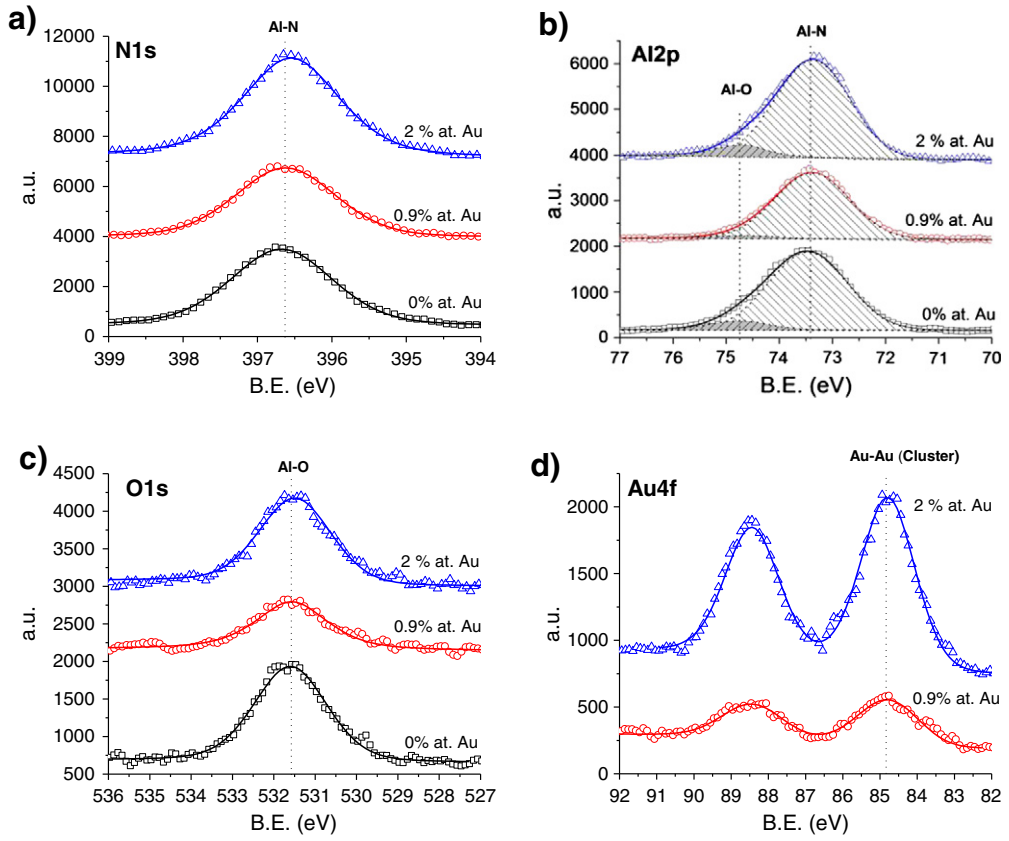

Fig. 6. XPS spectra of the as grown Au-AlN samples concerning the a) N 1s, b) Al 2p, c) O 1s, and d) Au 4f core levels. The experimental points are presented together with the fittings used for deconvolution (the Shirley background is not shown).

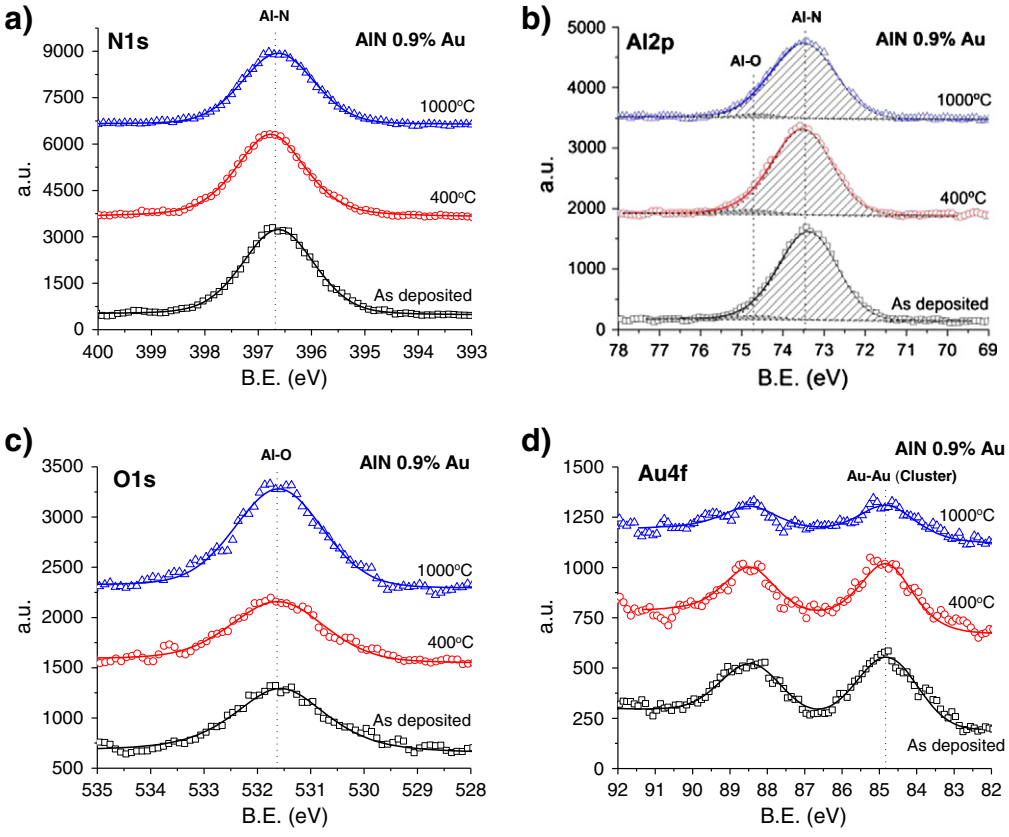

Fig. 7. XPS spectrums of the sample containing 0.9 at.% Au before and after two different thermal treatments, concerning the a) N 1s, b) Al 2p, c) O 1s, and d) Au 4f core levels. The experimental points are presented together with the fittings used for deconvolution (the Shirley background is not showed).

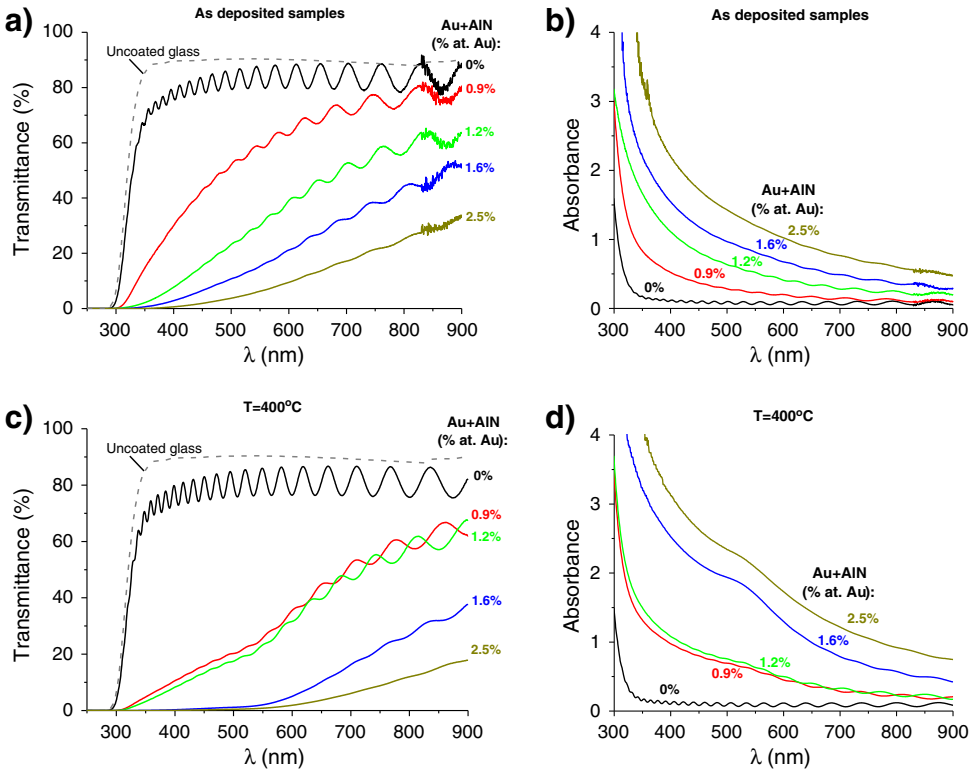

Fig. 8. Transmittance spectra of the Au + AlN nanocomposites a) before and c) after annealing at 400 °C; Absorbance spectra of the Au + AlN nanocomposites b) before and d) after annealing at 400 °C.

3.4. Optical properties

3.4.1. As-deposited samples

The optical transmittance was studied for both the as-deposited and 400 °C annealed samples (Fig. 8) in order to correlate the optical behaviour with the changes in the microstructure of the coatings suggested from the previous characterization techniques. A more convenient way of looking at these curves is to plot their corresponding absorbance curves ($Abs = -Log\ T$).

The pure AlN coating reveals an average transmission higher than 85% in the Vis-NIR range (Fig. 8a)). In comparison to stoichiometric AlN films, it is found that the transmittance cut-off is red shifted (see e.g. [2] for comparison). With the increase in the Au content the overall transmission of the coatings decreases markedly (Fig. 8a)), corresponding to an increase in the extinction coefficient; however, no SPR feature was present in the spectra of any of the as-deposited samples (Fig. 8b)). The absence of SPR absorption is in good agreement with the previous results and line of the discussion, confirming that the Au should exist under the form of atoms or very small precipitates (<0.5–1 nm) in the AlN matrix.

The optical constants (refractive index n and extinction coefficient k) of the as-deposited samples were estimated numerically from the transmittance results by means of an unconstrained optimization technique described in detail in [27] (Fig. 9a)). For the pure AlN sample the absorption coefficient (α) was also calculated from the extinction coefficient, via the equation $\alpha = 4\pi\kappa/\lambda$, where λ is the wavelength of the incident light. The α^2 law (valid for allowed direct transitions) provided a good fit to the experimental data, and by using a linear extrapolation technique the bandgap energy of the pure AlN + Au films was calculated.

The refractive index value of the pure AlN film (2.0) is in good agreement with those reported for aluminium nitride [28,29]. However, the optical gap for these films ($E_g = 4.1$ eV) is not as high as expected for a high quality AlN (e.g. [28,29]). Indeed, the relatively small value of the threshold energy indicates that the film contained a large number of structural defects, the energy levels of which most probably contributed to a narrowing of the gap. This is an expected result due to the formation of impurities like oxides. It is known that the cut-off wavelengths and the optical constants of AlN are strongly dependent on the oxygen incorporation. Lin et al. [28] studied the optical properties of AlON films and, with increasing oxygen content, they observed a decrease in the refractive index from 2.2 to 1.7 (at λ = 500 nm), and a decrease in the energy bandgap. The presence of point defects,

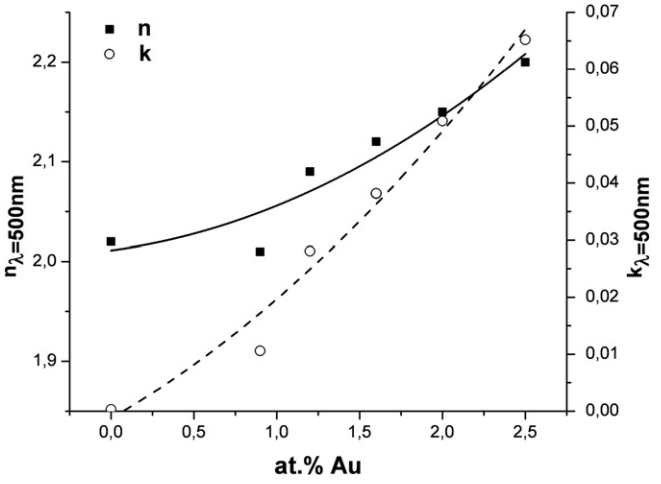

Fig. 9. Refractive index and extinction coefficient of the Au + AlN samples with different Au contents calculated from the transmittance curves (the trend lines are just a guide for the reader).

such as nitrogen vacancies or interstitials, may have occurred, as well as other defects in the boundaries of the polycrystalline grains, which could contribute to electron transitions. With the increase in the Au content both the refractive index and the coefficient of extinction were increased. For the maximum Au content (2.5 at.% Au) n and k values reached 2.2 and 0.065, respectively. The small gold agglomerates affect the electronic structure of the AlN phase by creating electronic states around the band edges, leading to a significant increase in the overall absorption but without the presence of any characteristic absorption peak.

Ellipsometry spectroscopy was performed to the as-deposited samples in order to try to validate the previous analysis. The optical properties of the AlN sample were obtained using a classical optical dispersion model (in the transparent region) and considering that the AlN is a uniaxial anisotropic material. A surface layer consisting of 50% film + 50% voids was also considered and its thickness was adjusted. The optical parameters of the silicon substrate were taken from the software database. Due to the strong absorption observed for the Au-AlN samples, the fitting for all samples was done only in the 1.5–3 eV energy range. There was no difference in the accuracy of the fitting if an Al_2O_3 layer was considered as part of the surface layer as mentioned by other authors.

The aluminium nitride sample without gold inclusion was clearly transparent up to 3.5 eV, energy above which a damping of the amplitude coming from the interference fringes was observed. As the gold content increases, the threshold energy for absorption moves to lower energies, suggesting a strong effect of the gold concentration in the electronic properties of the films. An example of the fitting can be seen in Fig. 10 for the pure AlN sample.

The final data of the ellipsometry analysis was compiled in Table 2. The values obtained by ellipsometry for the refractive index are close to the ones obtained by reverse analysis. Overall, it is observed that the refractive index is approximately constant, whereas the extinction coefficient increases with the Au content.

3.4.2. Annealed samples

After annealing at 400 °C, SPR absorption peaks appeared in the optical spectra of all the samples containing Au, resulting in an increased absorption (Fig. 8c) and d)). The Au resonance appeared centred around the 530 nm.

The absorbance curves were simulated making use of an effective medium theory. The Maxwell–Garnett (MG) model was chosen. Considering the classical MG approach, under the mean field approximation, the effective dielectric function ε_{eff} of the composite system containing a small volume fraction f of separate inclusions on a host medium is given by [30]:

$$\frac{\varepsilon_{eff}-\varepsilon_h}{\varepsilon_{eff}+2\varepsilon_h}=f\frac{\varepsilon_m-\varepsilon_h}{\varepsilon_m+2\varepsilon_h}$$

Table 2
Data obtained from the fitting of the ellipsometric spectra for the Au-AlN samples.

Ref.	t (μm)	At.% Au	SE			
			t (μm)	Ra (μm)	$(n, k)_E$	$(n, k)_O$
AlN-0	2.0	**0.0**	2.06	0.015	2.09, 0.006	2.06, 0.001
AlN-1	1.7	**0.9**	1.8	0.011	2.06, 0.007	2.04, 0.01
AlN-1.5	2.0	**1.6**	1.975	0.038	2.06, 0.074	2.05, 0.026
AlN-2	2.6	**2.0**	2.69	0.054	2.11, 0.07	2.09, 0.016

where ε_h is the dielectric function of the host medium and ε_m is the dielectric function of the metal inclusions.

To represent ε_{Au}, an analytical expression determined by Rakic et al. [31] based on the Brendel–Bormann (BB) model was used. In order to account for the intrinsic size effects of the nanoparticles, the BB model was modified by correcting the plasmon damping parameter (Γ) according to the equation [32]:

$$\Gamma=\Gamma_0+\frac{A\upsilon_F}{R}$$

where Γ_0 is the relaxation constant of the bulk metal (given in [31]), A is a phenomenological parameter that is a function of the geometry, of the order of unity (we used A = 0.8), υ_F is the Au Fermy velocity (1.39×10^{15} nm/s) and R is the radius of the nanoparticle (in nm).

After determining ε_{eff}, the optical properties of the nanocomposite thin films could be determined. For simulating light propagation in planar multilayer thin films, including the effects of multiple internal reflections and interference, the "Transfer Matrix Method" [32] was implemented in Mathematica. The absorbance of the system was then calculated through the relation $A = -Log\ T$.

An example of a simulation spectrum is shown in Fig. 11 for the sample containing the highest Au content.

In order to simulate the absorbance spectra of the 2.5 at.% AlN sample (Fig. 11), a thin layer of 100 nm consisting of 3 nm Au clusters surrounded by a medium consisting on a mixture of 20% of AlN and 80% of air (n = 1.2) was added to a thick homogenous layer of ~2000 nm with a dielectric constant similar to the one of the as-deposited 2.5 at.% AlN sample (calculated by reverse analysis). These results can suggest that at 400 °C the Au has segregated preferentially near the substrate where perhaps some microscopic buckling phenomenon has occurred (maybe due to the much lower coefficient of thermal expansion of glass when compared to silicon).

3.5. Hardness

The hardness values for crystalline AlN deposited on Si (111) are reported to be around 20 GPa [33], and in some cases even in the range 24–25 GPa [15]. For the as-deposited state, all Al–N + Au

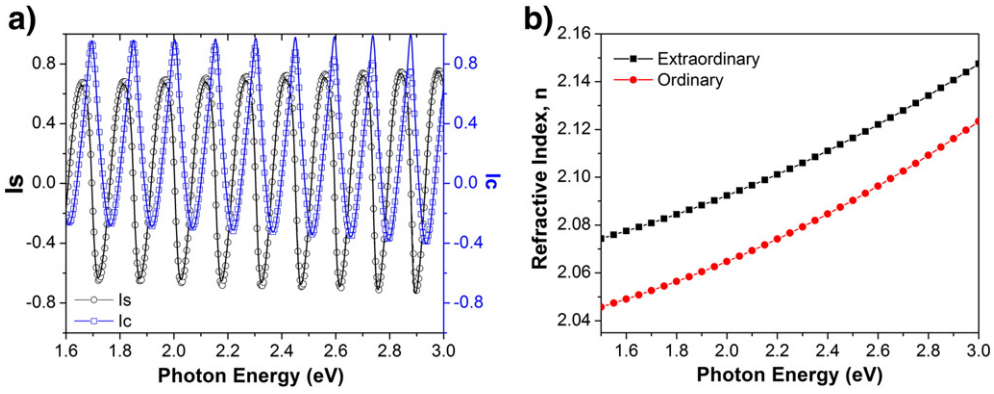

Fig. 10. a) Fitting obtained for the pure AlN sample, where the ordinary and extraordinary refractive indexes of the AlN thin film were extracted as shown in b).

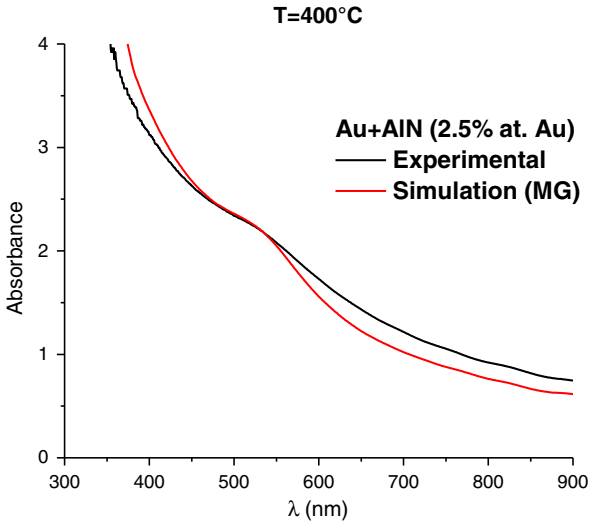

Fig. 11. Absorbance curve of the AlN sample containing 2.5 at.% Au together with the resulting simulation based on the MG approach.

coatings presented hardness values between 15 and 24 GPa, in good agreement with results from the literature (Fig. 12a)). For the coatings containing gold concentrations above 1.5 at.%, a steep decrease in the hardness was observed, from about 24 GPa down to the lowest value of 15 GPa for 2 at.%. Au. Several factors can be indicated for the decrease in the hardness values but no one is sufficiently strong to support the observed variation. The increase in Au content promotes: (1) an increase in the Al/N ratio which influences the structure orientation of the films; it is well known that two kinds of Al–N bond exist in wurtzite AlN, named B1 and B2. The (100) plane consist of only B1 bond, while (002), (102), (110) and (103) planes consist of B1 and B2 bonds together. The nature of the B1 bond is more covalent while that of the B2 is more ionic and its bond energy is relatively smaller than that of the B1 bond [20]. Therefore, when (100) planes are perpendicular to the surface they should be more resistant to indenter penetration giving rise to higher hardness. However, since glancing mode was used in the XRD analysis, preferential orientations are difficult to be analysed; (2) an increase of the Al–Au bonds in detriment of the strong Al–N covalent bond, with a possible decrease in the hardness; and (3) a more metallic character of the material with higher coefficients of thermal expansion (CTEs); as the coatings were deposited in a not cooled substrate holder, during the cooling down to room temperature a tensile stress component is added to the coating with the consequent decrease in the relative hardness.

For low Au content, there is a hardening factor that should be also considered, the solid solution hardening. The much higher atomic radius of Au in comparison with N can promote lattice distortion when Au atoms are isolated and replacing N in the AlN lattice. The induced local stresses can contribute for increasing the hardness of the material. The combination of these effects in a higher or lesser degree can determine the final hardness of the films. The reduced Young modulus values obtained, between 222 and 272 GPa, presented the same sharp decrease for samples containing more than 1.5 at.% Au (Fig. 12b)).

The annealing of the samples up to 300 °C did not change significantly the hardness. This is an expected result taking into account the temperature reached in the substrate holder during the deposition. Although temperatures were not measured, values in the range [250–350 °C] are estimated based on the experience of coating deposition onto different types of heat-treated steels. Thus, the coatings were already at that temperature before. For annealing at higher temperatures, stress relaxation is expected. During the cooling down to room temperature a new stress state can be introduced. Although as bulk materials Si and AlN have similar thermal expansion coefficients [34], Al–N in the form of thin film has higher values. The coefficient of thermal expansion of the Si(111) substrate is $\alpha_{Si} = 4 \times 10^{-6}/°C$ (determined experimentally) and for AlN thin films, reported values for the wurtzite structure are close to $\alpha_{\perp} = 5.3 \times 10^{-6}/°C$ and $\alpha_{\parallel} = 4.2 \times 10^{-6}/°C$ along the *a* and *c* axes, respectively [35]. Considering only the pure Al–N case, the major mismatch that could happen should be for samples with crystallites preferentially orientated with the (002) planes parallel to the substrate. Thus, tensile stresses should arise during cooling down. This situation would be further enhanced with the incorporation of Au, i.e. a progressively more metallic character (increased CTEs) will occur with increasing creation of tensile stresses. Therefore, a decrease in the hardness should occur after annealing.

For higher annealing temperatures (1000 °C) the coatings presented cracking, or even flaking off, due to the lack of adhesion of the films, hence not being suitable to be analysed properly by depth sensing indentation.

4. Conclusions

By varying the length of Au strips placed in the Al target and using a reactive atmosphere of N_2, Al–N coatings with different Au contents were deposited with maximum values up to 2.5 at.% Au. The extinction of the coatings increased remarkably when increasing the Au content. However, no SPR absorption peak was noted in any of the as-deposited samples. XRD and XPS confirmed that the Au should be embedded in the matrix in the form of very small nanoparticles (<0.5–1 nm) that can be so small as isolated atoms. The hardness of the coatings was high (~23 GPa) for the lowest Au concentrations, however it diminished for the highest Au contents. With temperature Au segregation in the matrix was obtained with the consequent appearance of the SPR

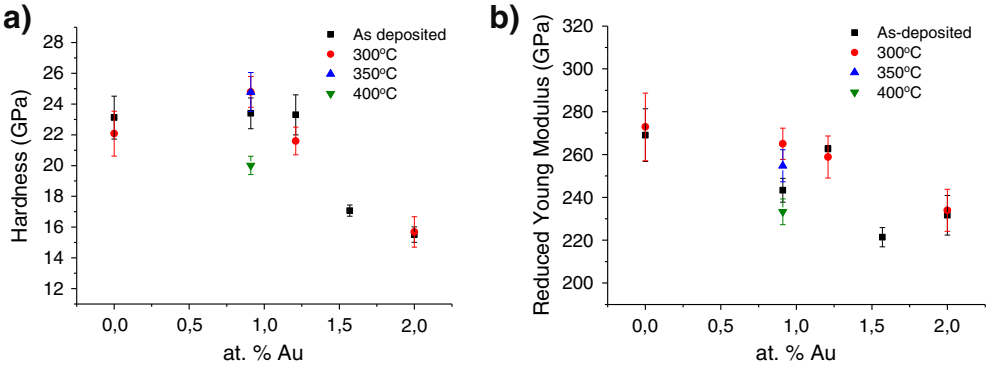

Fig. 12. a) Hardness and b) reduced modulus values for Al–N + Au samples, with increasing gold content, before and after annealing at increasing temperatures.

absorption peak in the visible spectrum. Different colorations were achieved both in the absence and in the presence of SPR features.

These films show a high potential for decorative applications, due to the high mechanical properties and chemical stability of the AlN. However, a few more studies need to be done in order to optimize the thermal stability of the nanocomposites.

Conflict of interest

None.

Acknowledgements

This research is co-sponsored by FEDER funds through the program programme COMPETE — *Programa Operacional Factores de Competitividade* - and by national funds through FCT — *Fundação para a Ciência e a Tecnologia*, under the projects CENTRO-07-0224 - FEDER-002001 (MT4MOBI) and DECOMAT: PTDC/CTM/70037/2006.

References

[1] G. Walters, I.P. Parkin, J. Mater. Chem. 19 (2009) 574–590.
[2] G. De, S. Bhattacharyya, J. Mater. Chem. 18 (2008) 2816–2824.
[3] J. Sasai, K. Hirao, J. Appl. Phys. 89 (2001) 4548.
[4] R.H. Magruder, L. Yang, R.F. Haglund, C.W. White, L. Yang, R. Dorsinville, R.R. Alfano, Appl. Phys. Lett. 62 (1993) 1730.
[5] J. Wang, W.M. Lau, Q. Li, J. Appl. Phys. 97 (2005) 114303.
[6] Y. Uemura, M. Iwata, Thin Solid Films 78 (1981) L55–L58.
[7] G.M. Matenoglou, H. Zoubos, A. Lotsari, C.E. Lekka, P. Komninou, G.P. Dimitrakopulos, C. Kosmidis, G.A. Evangelakis, P. Patsalas, Thin Solid Films 518 (2009) 1508–1511.
[8] A. Lotsari, G.P. Dimitrakopulos, T. Kehagias, P. Kavouras, H. Zoubos, L.E. Koutsokeras, P. Patsalas, P. Komninou, Surf. Coat. Technol. 204 (2010) 1937–1941.
[9] N.M. Figueiredo, C. Louro, R. Escobar Galindo, A. Climent-Font, A. Cavaleiro, Surf. Coat. Technol. 206 (2012) 2740–2745.
[10] K. Tominaga, H. Imai, Y. Sueyoshi, Surf. Coat. Technol. 61 (1993) 182–186.
[11] K. Wasa, S. Hayakawa, Handbook of Sputter Deposition Technology, Noyes Publications, New Jersey, 1992.
[12] B. Hvolbaek, T.V.W. Janssens, B.S. Clausen, H. Falsig, C.H. Christensen, J.K. Norskov, NanoToday 2 (2007) 14–18.
[13] N.M. Figueiredo, N.J.M. Carvalho, A. Cavaleiro, Appl. Surf. Sci. 257 (2011) 5793–5798.
[14] J.A. Thornton, Model. Opt. Thin Films 95 (1988) (Proc. SPIE 0821).
[15] T.A. Rawdanowicz, V. Godbole, J. Narayan, J. Sankar, A. Sharma, Compos. Part B 30 (1999) 657–665.
[16] S. Venkataraj, D. Severin, R. Drese, F. Koerfer, M. Wuttig, Thin Solid Films 502 (2006) 235–239.
[17] C. Duquenne, B. Popescu, P.-Y. Tessier, M.-P. Besland, Y. Scudeller, C. Brylinski, S. Delage, M.-A. Djouadi, Plasma Process. Polym. 4 (2007) S1–S5.
[18] E.J. Bienk, H. Jensen, G.N. Pedersen, G. Sorensen, Thin Solid Film 230 (1993) 121.
[19] A. Rodriguez-Navarro, W. Otaño-Rivera, J.M. García-Ruiz, R. Messier, L.J. Pilione, J. Mater. Res. 12 (1997) 1850.
[20] X.-H. Xu, H.-S. Wu, C.-J. Zhang, Z.-H. Jin, Thin Solid Films 388 (2001) 62–67.
[21] M. Ohring, Material Science of Thin Films, 2 edition Academic Press, 2001.
[22] http://www.icdd.com/.
[23] C.D. Wagner, W.M. Riggs, L.E. Davis, J.F. Moulder, G.E. Muilenberg, Handbook of X-ray Photoelectron Spectroscopy, Perkin-Elmer Corporation, Minnesota, 1978.
[24] D. Wolf, S. Yip, Materials Interfaces: Atomic-Level Structure and Properties, Chapman & Hall, London, 1992.
[25] I. Bertóti, Surf. Coat. Technol. 151–152 (2002) 194–203.
[26] X.-P. Kuang, H.-Y. Zhang, G.-G. Wang, L. Cui, C. Zhu, L. Jin, R. Sun, J.-C. Han, Superlattice. Microst. 52 (2012) 931–940.
[27] E.G. Birgin, I. Chambouleyron, J.M. Martínez, J. Comput. Phys. 151 (1999) 862–880.
[28] Y.-H. Lin, J.-C. Hsu, Y. Ding, P.W. Wang, Opt. Rev. 16 (2009) (400 [25]).
[29] H.C. Barshilia, B. Deepthi, K.S. Rajam, Thin Solid Films 516 (2008) 4168–4174.
[30] U. Kreibig, M. Vollmer, Optical Properties of Metal Clusters, Springer, Berlin, 1995.
[31] A.D. Rakic, A.B.. Djurišic, J.M. Elazar, M.L. Majewski, Appl. Opt. 37 (1998) 5271.
[32] O.S. Heavens, Optical Properties of Thin Solid Films, Dover Publications, New York, 1991.
[33] X.H. Ji, S.P. Lau, G.Q. Yu, W.H. Zhong, Y.G. Wang, B.K. Tay, J. Phys. D. Appl. Phys. 36 (2003) 2543–2547.
[34] H.O. Pierson, Handbook of Refractory Carbides and Nitrides, Noyes Publications, New Jersey, 1996.
[35] W.M. Yim, R.J. Paff, J. Appl. Phys. 45 (1974) 1456–1457.